Geophysical Journal International

Geophys. J. Int. (2012) doi: 10.1111/j.1365-246X.2012.05652.x

Surface wave eikonal tomography in heterogeneous media using exploration data

Pierre Gouédard,[1] Huajian Yao,[1,2] Fabian Ernst[3] and Robert D. van der Hilst[1]

[1] *Earth, Atmospheric and Planetary Sciences Department, Massachusetts Institute of Technology, 77 Massachusetts Avenue, Cambridge, MA 02139, USA. E-mail: gouedard@mit.edu*

[2] *Institute of Geophysics and Planetary Physics, Scripps Institution of Oceanography, UC San Diego, 9500 Gilman Drive, La Jolla, CA 92093, USA*

[3] *Shell Projects and Technology, Kessler Park 1, NL 2288 GS Rijswijk, the Netherlands*

Accepted 2012 August 16. Received 2012 June 4; in original form 2012 February 10

SUMMARY

Surface wave tomography often involves the construction of phase (or group) velocity maps through linearized inversion of measured phase (group) arrival times. Such inversions require *a priori* information about the medium (that is, a reference model) to calculate source–receiver paths as well as regularization. Surface wave eikonal tomography bypasses these limitations and has the advantage of being simple to implement and use, with virtually no input parameters. It relies on the accurate measurement of phase arrival time, which can be challenging for dispersive waves and complex waveforms. We present a measurement method based on the evaluation of phase arrival time differences at nearby receivers. We show, using an exploration data set, that the produced Rayleigh wave velocity maps are in agreement with results from traditional tomography. The latter reveals less detail, however, because of the regularization needed to accommodate for the heterogeneity of the study area and noise in the data. Eikonal tomography requires averaging over results from multiple sources to produce a proper image; for the scattering environment considered we estimate that a source spacing of 200 m is sufficient. Finally, we show that combining seismic interferometry and eikonal tomography is effective when the source coverage is inadequate.

Key words: Tomography; Interferometry; Controlled source seismology; Surface waves and free oscillations; Seismic tomography.

1 INTRODUCTION

Surface waves provide information about shallow structures and are of increasing interest in exploration geophysics, in particular for overburden characterization (e.g. Campman & Riyanti 2007; Socco & Boiero 2008). They are usually processed using a local layered medium approximation to obtain, in a first step, phase- or group-velocity maps for specific frequencies, which in a second step are then inverted into a *S*- (and sometimes *P*-) wave velocity model at shallow depth (e.g. Luo *et al.* 2008). The first step usually requires a ray tracer to compute traveltimes, which implies knowledge about the medium and about how waves propagate in the medium. In exploration seismology, this often reduces to the assumption of a homogeneous medium for which ray tracing is trivial. We present here a different approach to surface wave tomography: surface wave eikonal tomography, as initially proposed by Lin *et al.* (2009), combined with a neighbourhood-based cross-correlation method for phase arrival picking. This data-driven approach takes advantage of the high-density receiver arrays that are common in exploration seismics and can deal with complex media and waveforms. Eikonal tomography neither needs *a priori* information nor ray tracing (because it uses a local equation, the eikonal equation, to describe wave propagation) and has become possible for seismic exploration as recent technological advances made 2-D subwavelength spatial sampling feasible. It is easy to implement and it produces results that are robust and not dependent on the choice of input parameters. In a global seismology context, eikonal tomography has been successful in imaging crustal structure beneath western North America from ambient noise wavefields recorded using the EarthScope/USArray Transportable Array (Lin *et al.* 2009).

Measuring the phase arrival times that are used as input for this type of velocity analysis is challenging when working with waveforms that are complex owing to dispersion and scattering. Lin *et al.* (2009) built traveltime maps from (virtual) source–receiver phase measurements in narrow frequency bands. Direct measurement is efficient if the medium varies smoothly on a spatial scale that is (much) larger than the wavelengths of the waves considered, but it is not accurate in the presence of scattering and multipathing. To improve the quality of traveltimes measured from complex waveforms, we propose a traveltime picking algorithm that is based on the integration of delays between neighbouring receivers (obtained from cross-correlation).

In Section 2 of this paper, we present the theory of eikonal tomography and the phase measurement algorithm. In a second part, we apply surface wave eikonal tomography to data from a hydrocarbon exploration experiment for velocity analysis of a strongly heterogeneous and scattering medium. In Section 3, we use this data set for source depopulation—that is, we quantify the source spacing that is necessary to obtain a reliable velocity model for the area. Section 4 is devoted to validating joint seismic interferometry and eikonal tomography, which is useful when the coverage of active sources is not suitable for traditional eikonal tomography.

2 THEORY AND METHODS

2.1 Eikonal tomography

Traveltime tomography concerns the estimation of spatial variations in the propagation speed of seismic waves from a set of traveltimes of seismic phases between known source and receiver locations. Essentially, the traveltime is an integration (averaging) of the local wave slowness over the source–receiver paths:

$$t(\mathbf{r}_\mathrm{s}, \mathbf{r}_\mathrm{r}) = \int \frac{K(\mathbf{r}, \mathbf{r}_\mathrm{s}, \mathbf{r}_\mathrm{r})}{c(\mathbf{r})}\, \mathrm{d}\mathbf{r}, \tag{1}$$

where t is the traveltime from a source in position $\mathbf{r}_\mathrm{s}$ to a receiver in position $\mathbf{r}_\mathrm{r}$, $c(\mathbf{r})$ is the local structural phase wave speed (using the terminology introduced by Wielandt 1993) that we want to recover, and K is the integration kernel. The integration is done over 3-D space, but the spatial extent of the wave sensitivity depends on the theoretical approximations made: in the case of ray theory K vanishes everywhere except along the ray, whereas it is oscillatory (with non-zero values away from the ray) in the case of finite frequency wave theory (Dahlen *et al.* 2000; de Hoop & van der Hilst 2005). Traveltimes measurements are classically inverted, in a 'de-integration' operation, to map local phase velocity in the sampled area.

A different approach would be to use the hypereikonal equation (Beydoun 1985, also called frequency-dependent eikonal equation)

$$|\nabla t(\mathbf{r}_\mathrm{s}, \mathbf{r})|^2 = \frac{1}{c^2(\mathbf{r})} + \frac{\Delta A}{A\,\omega^2}, \tag{2}$$

which is derived from the Helmholtz equation (e.g. Wielandt 1993; Friederich *et al.* 2000). In (2), $\Delta = \nabla^2$ is the Laplacian, ω the angular frequency and A the amplitude of the waves. The latter includes source and receiver site effects and propagation effects (attenuation, scattering, interferences, ...). When using this equation to infer the local wave speed, the inversion process (if any) takes place when building the traveltime map, and not in a 'de-integration' step as in classical traveltime tomography. Note that for surface waves eq. (2) is an approximation as these waves do not, in general, obey the Helmholtz equation. It is valid, however, if we neglect mode conversions and the directivity of scattering from a point heterogeneity, which is justified as long as the medium can be considered locally homogeneous, that is, if it is only slightly or smoothly inhomogeneous compared to the heterogeneity of the wavefield (Friederich *et al.* 1993). The Helmholtz equation can be used for laterally heterogeneous media if the receiver network is dense enough to account for the interference among several plane waves and for the second spatial derivatives of the wavefield to be accurately estimated (Friederich *et al.* 2000). Pollitz & Snoke (2010) and Lin & Ritzwoller (2011) both developed imaging methods based on the Helmholtz equation, which they called, respectively, local non-planar surface wave tomography and Helmholtz tomography, and which they used to image the crust beneath western United States from earthquake surface wave data recorded at USArray.

The second term on the right-hand side of eq. (2), which accounts for finite frequency effects, can be neglected at high frequencies or if the amplitude of the propagating waves varies smoothly (e.g. in a slowly varying medium with simple illumination). This leads to the eikonal equation

$$|\nabla t(\mathbf{r}_\mathrm{s}, \mathbf{r})|^2 \approx \frac{1}{\hat{c}^2(\mathbf{r})}. \tag{3}$$

Here, $\hat{c}$ is a measure of wave speed that is affected by propagation effects (and in particular by the curvature of the wavefront and interference with other waves), and is therefore referred-to as the dynamic velocity (Wielandt 1993). We assume here that the dynamic velocity $\hat{c}$ equals the local structural velocity c used in (2), even though this is only true for plane waves (Friederich *et al.* 2000). Lin *et al.* (2009) developed and named the eikonal tomography method, based on eq. (3), and imaged the lithosphere of Western USA from ambient seismic noise.

In principle, the traveltime t (in eqs 2 and 3) needs to be known at each point of the study area, but the gradient can be computed with sufficient accuracy if t is known on the nodes of a dense grid (which is usually the case in seismic exploration). Any source and receiver geometry is suitable for this method, provided that the sensor spacing is sufficiently dense and realizing that interpolation may be needed to fill gaps in spatial sampling or to map the recording points onto a regular grid to ease the computation of the gradient.

Eq. (3) can be used to construct phase velocity maps for specific frequencies. In our study, we use it to produce phase velocity maps of the Rayleigh wave fundamental mode. In a second step, the dispersion curves at each location of the map could then be inverted for a local (shear wave) velocity profile as function of depth (Park *et al.* 1999; Socco & Strobbia 2004), and lateral juxtaposition of these depth profiles would then form (with interpolation, if necessary) 3-D volumes of shear wave speed. This second step requires *a priori* information about the medium and is not done here.

The above procedure is straightforward and easy to implement, but we make a few comments. First, we note that the pointwise inversion for local shear wave speed profiles (that is, the second step) renders the mapping between data and structure essentially asymptotic. Second, consideration of azimuthal anisotropy is straightforward, as shown by Lin *et al.* (2009, 2011b). Indeed, the vectorial form of eq. (3) leads directly to the wave vector $\mathbf{k}_\mathrm{s}(\mathbf{r}) = \left(\omega/\hat{c}_\mathrm{s}(\mathbf{r})\right) \mathbf{u}_\mathrm{s}(\mathbf{r})$, where $\mathbf{u}_\mathrm{s}(\mathbf{r})$ is the local propagation direction at point $\mathbf{r}$ for a source at $\mathbf{r}_\mathrm{s}$, and $c_\mathrm{s}(\mathbf{r})$ is the local velocity at this point and for this direction. Keeping track of both the norm and the direction of $\mathbf{k}_\mathrm{s}$ ($\mathbf{u}_\mathrm{s}$ being different for each source position) allows getting velocity-versus-azimuth plots at each pixel of the final map, which usually gives the information about azimuthal anisotropy. Because of limitations of the data set, however, we did not consider this possibility in this paper. Third, the eikonal tomography can also be used for other surface wave modes (including Love waves if two horizontal components of the wavefield are available) or for body waves (provided that t can be measured on a 3-D grid, which is not usually the case).

2.2 Phase arrival time measurements

Taking the gradient is a numerically unstable operation and measuring the phase arrival times must be done with great care to ensure a

smooth traveltime map. The dispersive nature of the surface waves used in this study makes it difficult to define the arrival time. Moreover, scattering can produce complex waveforms (as is the case in our study) making it difficult to track individual phases. To address these observational challenges, we propose a neighbourhood-based cross-correlation method to measure arrival time differences between nearby receivers. This method is similar to the multichannel cross-correlation method (Vandecar & Crosson 1990), in which each trace is cross-correlated with all other traces to obtain the relative time-shifts, but in this study we limit the correlation to nearby stations to avoid cycle-skipping and ensure waveform similarity. For each source s, the relationship between the arrival time differences between the receivers and the source–receiver traveltimes can be written

$$\mathbf{D}\,\mathbf{t}^{\mathrm{s}} = \Delta\mathbf{t}^{\mathrm{s}}, \tag{4}$$

where $\mathbf{D}$ is a differentiation matrix (a sparse matrix with one '+1' and one '−1' per line) of size $N_{\mathrm{r}} \times N_{\mathrm{r}}(N_{\mathrm{r}}-1)/2$ (N_{r} being the number of receivers), $\mathbf{t}^{\mathrm{s}} = (t_i^{\mathrm{s}})_{i=1\ldots N_{\mathrm{r}}}$ is the vector of traveltimes at each receiver, and $\Delta\mathbf{t}^{\mathrm{s}} = (\Delta t_{ij}^{\mathrm{s}} = t_j^{\mathrm{s}} - t_i^{\mathrm{s}})_{i=1\ldots N_{\mathrm{r}},\ j=1\ldots N_{\mathrm{r}}}$ is the vector of measured arrival time differences between receivers, from cross-correlation of narrow-band filtered (fundamental mode) surface waves. The number of pairs of receivers considered may vary, depending on data quality and medium heterogeneity, but as mentioned earlier we limit ourselves to the closest neighbours. The measurement error on $\Delta\mathbf{t}^{\mathrm{s}}$ is evaluated as the width of the 90 per cent confidence interval from the correlation of waveforms.

Eq. (4) describes a Bayesian problem, which can be solved with a quasi-Newton method (e.g. Tarantola 2005)

$$\mathbf{t}^{\mathrm{s}} \approx \tilde{\mathbf{D}}^{-1}\,\Delta\mathbf{t}^{\mathrm{s}}, \tag{5}$$

where $\tilde{\mathbf{D}}^{-1}$ is the pseudo-inverse of the differentiation matrix $\mathbf{D}$ (that is, $\tilde{\mathbf{D}}^{-1}$ is an integration matrix), which can be written as

$$\tilde{\mathbf{D}}^{-1} = \left(\mathbf{D}^{\mathrm{T}}\,\mathbf{C}_{\mathrm{D}}^{-1}\,\mathbf{D} + \mathbf{C}_{\mathrm{M}}^{-1}\right)^{-1}\,\mathbf{D}^{\mathrm{T}}\,\mathbf{C}_{\mathrm{D}}, \tag{6}$$

where $\mathbf{D}^{\mathrm{T}}$ denotes the transpose of $\mathbf{D}$, $\mathbf{C}_{\mathrm{D}}$ is a data covariance matrix, and $\mathbf{C}_{\mathrm{M}}$ is a model covariance matrix. For $\mathbf{C}_{\mathrm{D}}$, we use a diagonal matrix which elements are proportional to the measurement error in $\Delta\mathbf{t}$. Regularization is introduced by choosing a second-order differentiation matrix for $\mathbf{C}_{\mathrm{M}}^{-1}$. This definition of the covariance matrix ensures a traveltime map close to the one expected for a homogeneous model (the second derivative of the traveltime with respect to the distance is zero).

As $\tilde{\mathbf{D}}^{-1}$ is an integration operator, $\mathbf{t}^{\mathrm{s}}$ is defined modulo a constant of integration. This ambiguity could be resolved by extrapolating the traveltime $\mathbf{t}^{\mathrm{s}}$ towards zero offset, where it has to be zero, but this is difficult in practice because traveltime measurements at short offsets from the source (within one or two wavelengths) are not reliable due to near-field effects. The value of the integration constant is irrelevant, however, because we are only interested in the gradient of $\mathbf{t}^{\mathrm{s}}$ (see eq. 2).

Eqs (3) and (5) may suggest that our approach is equivalent to double-difference tomography (Zhang & Thurber 2003). It is different, however, because we do not have to include any *a priori* information, such as a starting model and we do not have to trace any rays because the ray information is naturally included in the gradient from eq. (2). For a more complete discussion on how rays are handled in eikonal tomography, we refer to Lin *et al.* (2009).

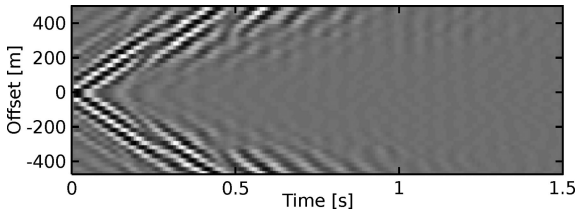

Figure 1. A shot gather, bandpass filtered between 10 and 20 Hz, illustrating the complexity of the waveform. The amplitude is normalized.

3 APPLICATION FOR SHALLOW SUBSURFACE IMAGING

3.1 Data and pre-processing

For our study, we use data from a high-resolution survey of a 1 km × 1 km carbonate (karst) area in northern Oman conducted by Petroleum Development Oman (PDO). Receiver points are located at the nodes of a 40 × 40 grid (25 m × 25 m spacing). Each receiver point consists of a group of 12 vertical geophones, from which data are stacked onsite. Sources are vibrator trucks acting at the nodes of a similar grid, shifted with respect to the receiver grid by half a grid distance in both directions (that is, 12.5 m). Records are 4 s long and the sampling frequency is 125 Hz. For a more complete description of the data set, we refer to Herman & Perkins (2006) and Gouédard *et al.* (2008). Fig. 1 illustrates the complexity of the waveforms produced by scattering.

The complete data set consists of 1600 × 1600 vertical component source–receiver time-domain signals and constitutes an exhaustive measurement of the transfer functions of the half-space medium over a 1-km^2 area. Because of the 2-D acquisition geometry, the data set includes mainly Rayleigh waves.

Records are first filtered around the different working frequencies using a Gaussian filter of 10 per cent width. The central frequencies considered in the following are 10, 15 and 20 Hz. The filtered waveforms are then windowed in time around the maximum of the envelope, effectively extracting the fundamental-mode Rayleigh wave in this small-scale set-up.

3.2 Inversion and discussion

To account for possible data quality reduction due to noise when using real data, we subjected the measured traveltime differences $\Delta\mathbf{t}$ to quality control. The correlation-based approach that we used to measure $\Delta\mathbf{t}$ assumes that the recorded waveforms are similar between neighbours. We thus used the correlation coefficient between these waveforms, windowed around the fundamental-mode Rayleigh wave, as a quality criterion. We choose a threshold value of 0.98 for this correlation coefficient, and measurements with smaller values are not considered. This procedure typically rejects 30 per cent of the measurements for each source. This data selection helps stabilize the inversion for a single source, but when results from different sources are stacked this selection is not critical because the implied averaging smooths out the outliers in single-source velocity models. For instance, lowering the threshold value to 0.9 results in the rejection of less than 0.5 per cent of the measurements but produces a final velocity map that differs by less than 0.5 per cent (on a per-pixel basis) from the one presented later in this paper.

Eq. (2) (or 3) can be used to produce maps of the structural (or dynamic) velocity from a single source (Fig. 2). Subsequently, phase velocity maps from all sources can be combined, which leads to the

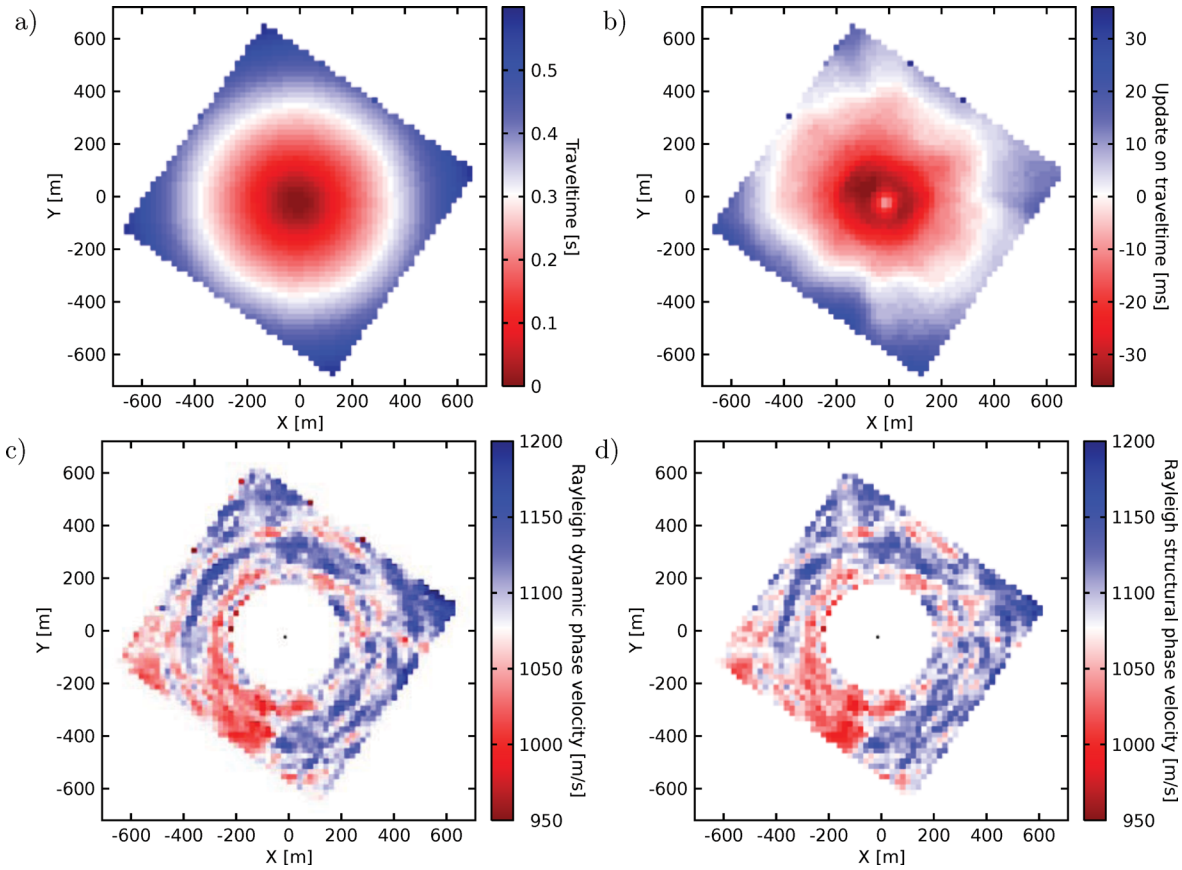

Figure 2. (a) Traveltime map for the fundamental-mode Rayleigh wave at 15 Hz, for one source located at the centre of the array. (b) Same as (a), but with the mean gradient (1187 m s^{-1}) removed to emphasis differences with an homogeneous medium (for illustration purposes only, not used in the inversion). (c) Dynamic phase velocity map for this source, obtained from the spatial gradient of the map in (a), following eq. (3). The source location is indicated by the black dot in the centre of the array. Offsets smaller than 200 m are omitted because of their unreliability due to near-field effects (Lin *et al.* 2009). (d) Structural phase velocity map for this source, obtained following eq. (2).

velocity maps presented in Figs 3(a) and (b) for average dynamic and structural velocities, respectively.

Structural velocity is preferred, as it represents a medium property, but the calculation of the dynamic velocity is easier and numerically more stable because it avoids the calculation of the second derivative and division by the amplitude. Moreover, eq. (2) is not easy to use because the recorded Rayleigh wave amplitudes are not always meaningful or accurate. In our data set, for instance, the records are not from single receivers but from groups of 12 receivers so that the original amplitudes are not retained. Given the size of the groups (25 m) and the wavelengths of interest (>70 m), and because the signals represent simple sums of traces recorded at each geophone within a group, it is expected that the relative amplitude information is maintained for this data set. Figs 2 and 3 demonstrate that the differences between the two velocities are small and do not have spatial structure, which justifies the use of the dynamic velocity (which avoids the above-mentioned issues with amplitude). This might not always be the case, however, as discussed by Lin & Ritzwoller (2011) in the context of a regional to continental-scale study (with lower frequencies).

Fig. 3(a) presents the Rayleigh wave phase velocity at 15 Hz, and results for two other frequencies are presented in Figs 4(a) and (b). These maps reveal strong medium heterogeneity. This heterogeneity would complicate any tomography based on ray tracing, such as traditional or double-difference tomography, and it is likely that in such applications much of the structural details inferred here would have been lost due to regularization. We note that the averaged slowness values at each frequency match the values found by Gouédard *et al.* (2011, fig. 2) for a laterally homogeneous equivalent medium for this area. The observed increase of velocity with increasing frequency could be a bias due to scattering (Kaelin & Johnson 1998) or represent a real depth variation in average wave speed—and, hence, material properties—with depth.

Eikonal tomography allows the estimation of uncertainties in local wave speed through statistical comparison of values obtained from the inversion of data from different sources (Lin *et al.* 2009). Fig. 5 presents velocity uncertainties at 10, 15 and 20 Hz, associated with the velocity maps of Figs 3(a), 4(a) and (b), respectively. This shows that for each frequency the velocities estimates are less reliable on the eastern part of the array. The uncertainties are lowest at 15 Hz; at 20 Hz they are higher but remain below the main velocity contrasts of Fig. 4(b). Anisotropy (not included in the analysis here) could explain part (but not all) of the uncertainty. Other sources of uncertainty are noisy data or amplitude effects neglected in eq. (3), such as contamination by scattered surface waves (especially at higher frequencies).

We recall that a 3-D velocity model can be obtained from velocity maps such as presented in Fig. 4 (but then calculated for a range of frequencies) through pointwise inversion of the (fundamental-mode Rayleigh wave) dispersion curve for a *S*- and *P*-wave velocity profile with depth (e.g. Socco & Strobbia 2004; Luo *et al.* 2008). This requires *a priori* information about the medium (to calculate the

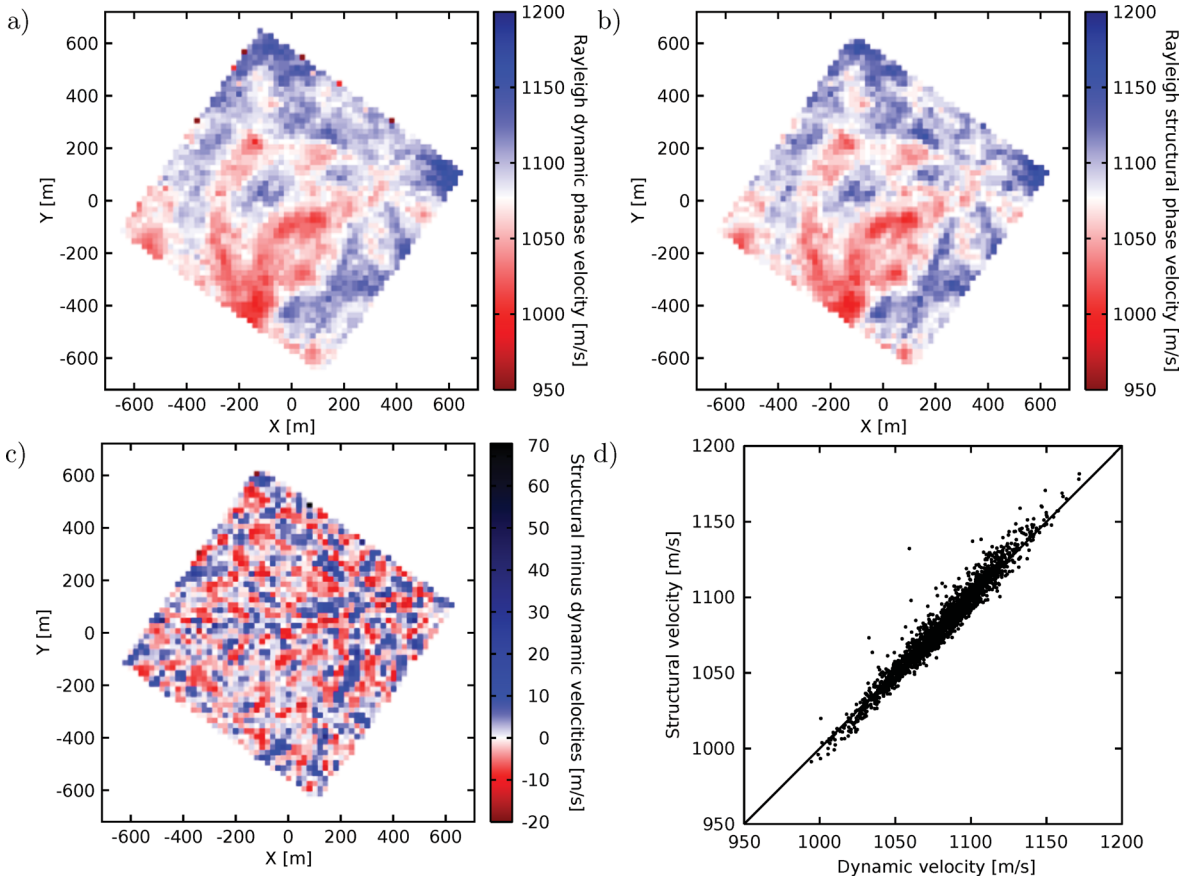

Figure 3. Comparison of the Rayleigh wave fundamental-mode (a) dynamic and (b) structural phase velocity maps, at 15 Hz. (c) Difference of the two maps (structural minus dynamic). (d) Cross-plot of the dynamic and structural velocities for each pixel.

proper sensitivities to relate dispersion to elastic medium properties at different depths) and is not done here.

In Fig. 4(c), we show the group-velocity model obtained by Gouédard *et al.* (2011) from the same data. Gouédard *et al.* (2011) used a traveltime tomography approach to produce a fundamental-mode Rayleigh wave group-velocity map (as opposed to phase velocity here) in a broader frequency band (10–25 Hz, but with a dominant frequency around 12 Hz) than considered here. Despite the differences in inversion method, frequency content and wave type, the results are consistent: while the tomography result is smoother due to regularization and the use of lower frequency data, the main structures of Figs 3(a), 4(a) and (b) are also present in Fig. 4(c). We also verified (not shown here) that approximating the group slowness with the frequency derivative of the phase slowness times the frequency yields a map close to the one displayed in Fig. 4(c). This comparison shows that, as expected, eikonal tomography yields higher resolution maps.

3.3 Source depopulation: how many sources are necessary?

Averaging over multiple sources suppresses the effects of wave propagation (due to medium heterogeneity) on the estimation of dynamic velocity from eq. (3) (Friederich 1998). A question that immediately arises is how many sources are actually necessary to recover a good velocity model. To address this question, we conducted a source depopulation exercise by considering fewer and fewer sources in the averaging process, as illustrated by Fig. 6. Note that Fig. 2(c) completes the series, with only one source located at the centre of the image area. To assess the quality of model reconstruction, we compare the obtained velocity models to the one obtained using all available sources (Fig. 4b), which we assume to be the best possible recovery of the medium fundamental-mode Rayleigh wave velocity. The comparison is done by computing the correlation coefficient R between the value of the velocity at each pixel. Table 1 shows that using 25 sources instead of the 1600 available (200 m spacing instead of 25 m) degrades the result only slightly. An *a posteriori* comparison of Figs 4(b) and 2(c) also shows that, despite having more artefacts, the map obtained with only one source already includes the main features of the final map.

4 INTERFEROMETRY

We discussed earlier how averaging over sources helps to get a reliable velocity model. Another practical limitation comes from the source distribution, that is, the actual location of these sources. Even though, in theory, any source/receiver geometry is suitable for the technique to work (as long as the receiver array is sufficiently dense), in practice only a limited range of source–receiver offsets can be used. Traveltime measurements in the near field of the sources are not reliable, as illustrated by Fig. 2, which defines the short offset limit [we note that the 200 m minimum offset used here is consistent with the three-wavelength criterion advocated by Lin *et al.* (2009)]. At offsets that are too large, poor signal-to-noise ratio prevents the traveltime differences between neighbours to be measured

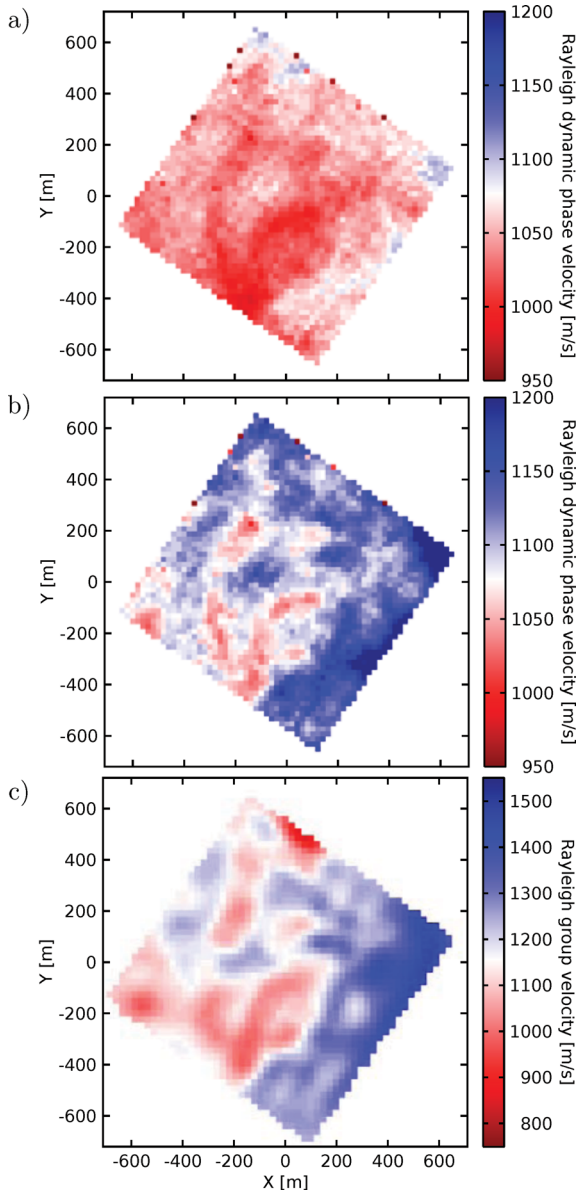

Figure 4. Rayleigh wave phase-velocity maps obtained from eikonal tomography at (a) 10 Hz; and (b) 20 Hz. (c) Rayleigh wave fundamental-mode group velocity in the 10–25 Hz frequency band (with a dominant frequency around 12 Hz) obtained using traveltime tomography (from Gouédard *et al.* 2011).

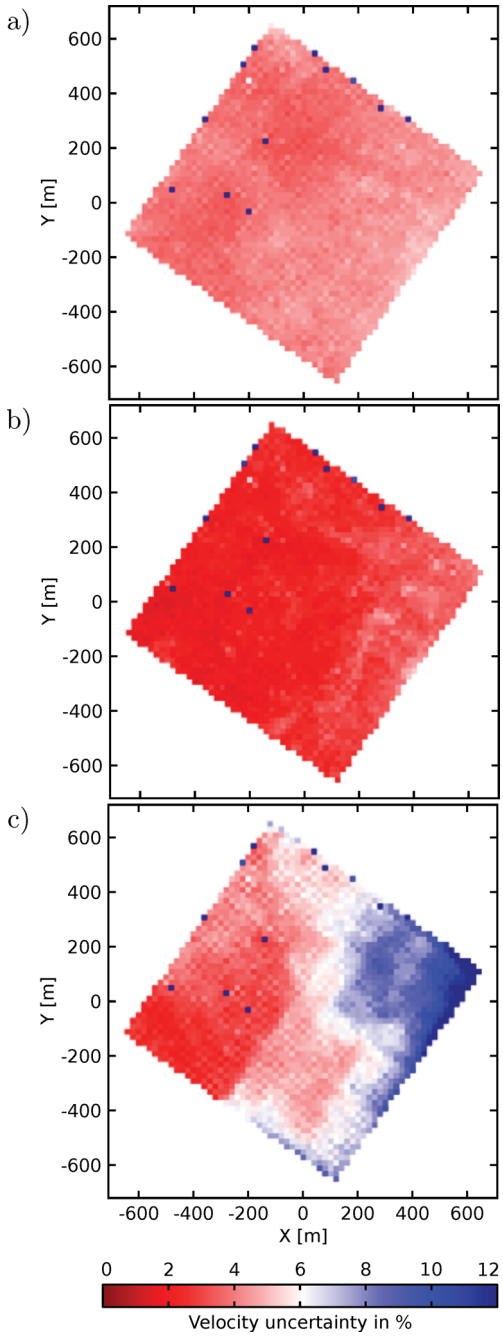

Figure 5. Velocity uncertainties at (a) 10 Hz, (b) 15 Hz and (c) 20 Hz, associated with the velocity maps of Figs 3(a), 4(a) and (b), respectively.

accurately. These practical limits can obstruct the construction of velocity maps for the whole array.

It is well established that (under appropriate conditions) cross-correlation of a wavefield recorded at two receivers approximates the Green's function for waves propagating between them, (e.g. Campman *et al.* 2005; Gouédard *et al.* 2008, 2011, for applications in a prospecting context). This technique, usually referred-to as seismic interferometry, allows one to have a virtual source at any of the receiver locations. In the context of this paper, it allows the transformation of the source–receiver geometry constraints to receiver–receiver constraints, which are easier to satisfy thanks to the dense receiver array.

The interferometric workflow is similar to the one presented earlier, but preceded by the Green's function reconstruction. This step consists in considering pairs of receivers and averaging the cross-correlation of records at each receiver over a distribution of sources. Following the discussion in Gouédard *et al.* (2008), we chose to consider sources in the alignment of the receiver pair (the so-called endfire lobes). This ensures a good reconstruction of direct waves, even if only a few sources are recorded by the two receivers, and also avoids inappropriate azimuthal energy distribution in the wavefield. The cross-correlation functions are then symmetrized by stacking their positive- and negative-time sides. The reconstructed Green's functions are used as an input to eikonal tomography, as if a source was located at one of the receivers. The resulting maps, at the same frequencies as used before, are presented in Fig. 7. These maps are comparable to those from Fig. 4, which demonstrates the feasibility

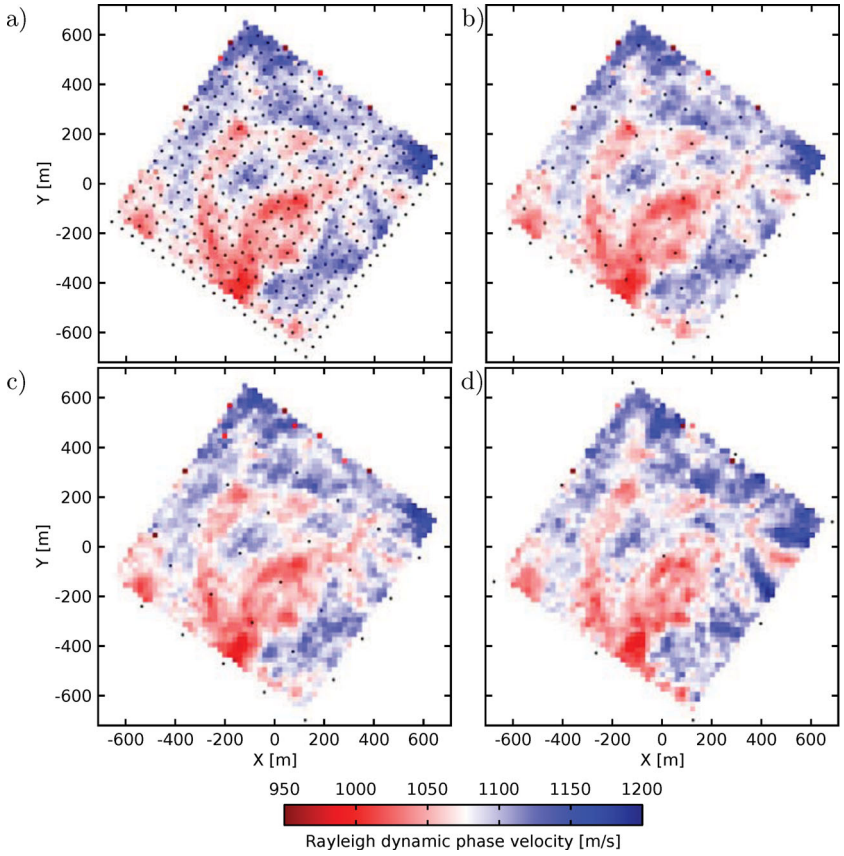

Figure 6. Source depopulation at 15 Hz. Maps are obtained by using less sources than the 1600 available involved to produce Fig. 4(b). The number of sources (which locations are indicated by the black dots) used for each figure is as follow: (a) 400 sources (one over two in both directions); (b) 100 sources (one over four in both directions); (c) 25 sources and (d) nine sources. Fig. 2(c) completes the series with only one source used.

Table 1. Correlation coefficients R between the Rayleigh wave phase velocity maps obtained by decreasing the number of sources, and the map obtained using the 1600 available sources.

No. of sources	400	100	25	9	1
R	0.9995	0.9926	0.9612	0.8542	0.7285

of interferometric eikonal tomography, using active source, similar to using seismic ambient noise (Lin *et al.* 2009).

We note that interferometric reconstruction of the amplitude of the Green's functions is still a topic of research and is not guaranteed in a general set-up and processing workflow (Gouédard *et al.* 2008; Cupillard & Capdeville 2010; Lin *et al.* 2011a), and only dynamic velocities can be obtained using this approach.

5 CONCLUSIONS

We propose an alternative approach to imaging subsurface from surface waves, namely surface wave eikonal tomography (combined with a neighbourhood-based cross-correlation method for traveltime measurement), which overcomes some important limitations of traveltime tomography, that is, the need of *a priori* information about medium heterogeneity and loss of short-wavelength structure due to regularization. Our approach takes advantage of the high density of receiver arrays, which allows the use of a local equation to link traveltime and phase velocity (instead of the integral relationship used for traveltime tomography), is easy to implement and use, and it does not require *a priori* information (e.g. a starting model).

We showed that, at least in the wavenumber ranges used in this study, dynamic phase velocity can effectively replace structural phase velocity, making the inversion numerically more stable and the results more robust since amplitude information is not always accurately preserved during pre-processing.

Surface wave eikonal tomography requires a dense receiver array as well as numerous sources. We studied the effect of reducing the number of sources, in a source-depopulation exercise, and showed that (for the medium used in our study) a 200-m source spacing is sufficient to produce an adequate image. When source coverage is not adequate, either in terms of spatial distribution or number of sources, seismic interferometry can produce virtual records that can be used as input for eikonal tomography.

ACKNOWLEDGMENTS

The authors thank the Ministry of Oil and Gas of the Sultanate of Oman, Petroleum Development of Oman and Shell Research for permission to use the data and publish these results. The authors are also grateful to Arie Verdel, formerly at Shell, and now at TNO Geological Survey of the Netherlands, for his help in starting this project, and for the stimulating discussions that followed. PG is supported by a Shell Research grant.

Lastly, we thank the editor, Prof Jean Virieux, and the three anonymous reviewers for their comments and suggestions which improved this manuscript.

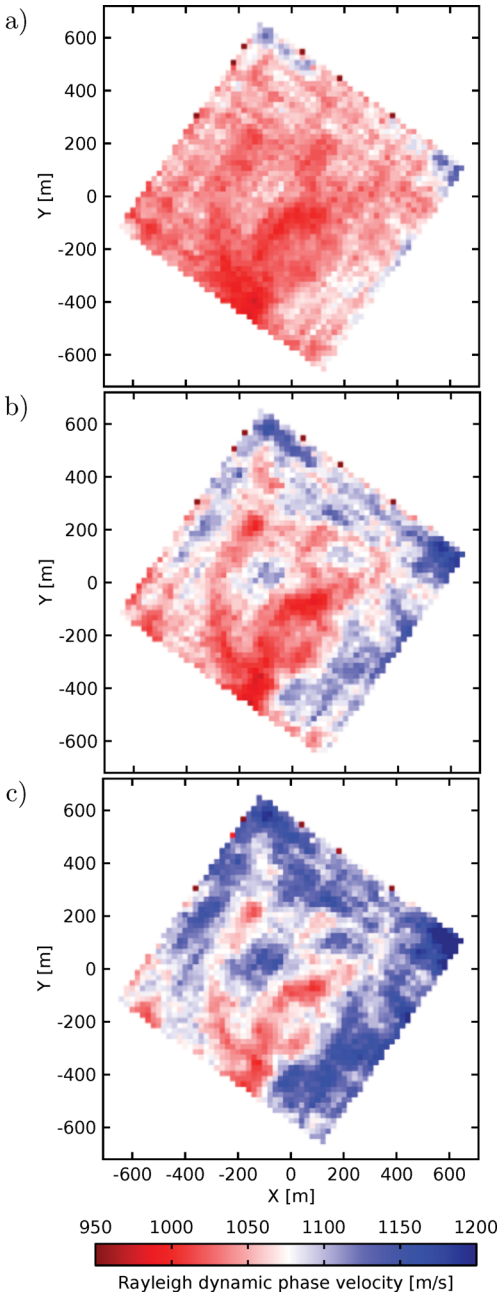

Figure 7. Same as Figs 3(a), 4(a) and (b), but from eikonal tomography applied to reconstructed Green's functions obtained with controlled sources seismic interferometry. As a reminder, the considered frequency bands are: (a) 10 Hz; (b) 15 Hz and (c) 20 Hz.

REFERENCES

Beydoun, W.B., 1985. Asymptotic wave methods in heterogeneous media, *PhD thesis*, Massachusetts Institute of Technology. Available at http://hdl.handle.net/1721.1/51449 (last accessed 2012 September 3).

Campman, X. & Riyanti, C.D., 2007. Non-linear inversion of scattered seismic surface waves, *Geophys. J. Int.,* **171**(3), 1118–1125.

Campman, X.H., van Wijk, K., Scales, J.A. & Herman, G.C., 2005. Imaging and suppressing near-receivers scattered surface waves, *Geophysics,* **70**(2), V21–V29.

Cupillard, P. & Capdeville, Y., 2010. On the amplitude of surface waves obtained by noise correlation and the capability to recover the attenuation: a numerical approach, *Geophys. J. Int.,* **181**(3), 1687–1700.

Dahlen, F.A., Hung, S.-H. & Nolet, G., 2000. Fréchet kernels for finite-frequency traveltimes—I.Theory, *Geophys. J. Int.,* **141**(1), 157–174.

de Hoop, M.V. & van der Hilst, R.D., 2005. On sensitivity kernels for 'wave-equation' transmission tomography, *Geophys. J. Int.,* **160**(2), 621–633.

Friederich, W., 1998. Wave-theoretical inversion of teleseismic surface waves in a regional network: phase-velocity maps and a three-dimensional upper-mantle shear-wave-velocity model for southern Germany, *Geophys. J. Int.,* **132**(1), 203–225.

Friederich, W., Wielandt, E. & Stange, S., 1993. Multiple forward scattering of surface waves: comparison with an exact solution and Born single-scattering methods, *Geophys. J. Int.,* **112**(2), 264–275.

Friederich, W., Hunzinger, S. & Wielandt, E., 2000. A note on the interpretation of seismic surface waves over three-dimensional structures, *Geophys. J. Int.,* **143**(2), 335–339.

Gouédard, P., Roux, P., Campillo, M. & Verdel, A., 2008. Convergence of the two-point correlation function toward the Green's function in the context of a seismic prospecting data set, *Geophysics,* **73**(6), V47–V53.

Gouédard, P., Roux, P., Campillo, M., Verdel, A., Yao, H. & van der Hilst, R.D., 2011. Source depopulation potential and surface wave tomography using a crosscorrelation method in a scattering medium, *Geophysics,* **76**(2), SA51–SA61.

Herman, G.C. & Perkins, C., 2006. Predictive removal of scattered noise, *Geophysics,* **71**(2), V41–V49.

Kaelin, B. & Johnson, L., 1998. Dynamic composite elastic medium theory. Part II. Three-dimensional media, *J. appl. Phys.,* **84**(10), 5458–5468.

Lin, F.-C. & Ritzwoller, M.H., 2011. Helmholtz surface wave tomography for isotropic and azimuthally anisotropic structure, *Geophys. J. Int.,* **186**(3), 1104–1120.

Lin, F.-C., Ritzwoller, M.H. & Snieder, R., 2009. Eikonal tomography: surface wave tomography by phase front tracking across a regional broad-band seismic array, *Geophys. J. Int.,* **177**(3), 1091–1110.

Lin, F.-C., Ritzwoller, M.H. & Shen, W., 2011a. On the reliability of attenuation measurements from ambient noise cross-correlations, *Geophys. Res. Lett.,* **38,** L11303, doi:10.1029/2011GL047366.

Lin, F.-C., Ritzwoller, M.H., Yang, Y., Moschetti, M.P. & Fouch, M.J., 2011b. Complex and variable crustal and uppermost mantle seismic anisotropy in the western United States, *Nature Geosci.,* **4**(1), 55–61.

Luo, Y., Xia, J., Liu, J., Xu, Y. & Liu, Q., 2008. Genration of a pseudo 2D shear-wave velocity section by inversion of a series of 1D dispersion curves, *J. appl. Geophys.,* **64**(3–4), 115–124.

Park, C.B., Miller, R.D. & Xia, J., 1999. Multichannel analysis of surface waves, *Geophysics,* **64**(3), 800–808.

Pollitz, F.F. & Snoke, J.A., 2010. Rayleigh-wave phase-velocity maps and three-dimensional shear velocity structure of the western US from local non-plane surface wave tomography, *Geophys. J. Int.,* **180**(3), 1153–1169.

Socco, L.V. & Boiero, D., 2008. Improved Monte Carlo inversion of surface wave data, *Geophys. Prospect.,* **56**(3), 357–371.

Socco, L.V. & Strobbia, C., 2004. Surface-wave method for near-surface characterization: a tutorial, *Near Surf. Geophys.,* **2**(4), 165–185.

Tarantola, A., 2005. *Inverse Problem Theory and Methods for Model Parameter Estimation,* Society for Industrial and Applied Mathematics, Philadelphia, PA.

Vandecar, J.C. & Crosson, R.S., 1990. Determination of teleseismic relative phase arrival times using multi-channel cross-correlation and least squares, *Bull. seism. Soc. Am.,* **80**(1), 150–169.

Wielandt, E., 1993. Propagation and structural interpretation of non-plane waves, *Geophys. J. Int.,* **113**(1), 45–53.

Zhang, H. & Thurber, C.H., 2003. Double-difference tomography: the method and its application to the Hayward Fault, California, *Bull. seism. Soc. Am.,* **93**(5), 1875–1889.